3D AVO Processing: A Case Study from the Gulf of Mexico

N. Moldoveanu, M K. Sengupta*, Schlumberger ,D.R. Andress, V. Kriechbaum

Kerr McGee Corp

SUMMARY

3D AVO is one of the emerging seismic technologies that is now being used more and more, as a tool for hydrocarbon exploration and field development. A key component of this technology is the 3D pre-stack processing for AVO. The improvements made in the past few years in preserving the seismic amplitudes in the 3D pre-stack processing sequence give more confidence in the resultant AVO analysis. The purpose of this paper is to illustrate the effects of a carefully executed 3D AVO processing on a data set acquired by Schlumberger Geco–Prakla over a High Island prospect in the Gulf of Mexico. The results of this 3D AVO processing and analyses were confirmed by the drilling of a successful discovery well.

INTRODUCTION

In 1989, several 2D seismic lines were acquired over a High Island prospect in the Gulf of Mexico, and these 2D lines showed high amplitude anomalies that could be prospective targets for exploration. AVO processing was performed by on one of the 2D lines, but it did not validate the amplitude anomalies to be due to hydrocarbons. Subsequently, a non-exclusive proprietary (NEPS) 3D seismic survey was acquired by Schlumberger Geco-Prakla in 1995-1996 over this High Island prospect. Oryx Energy Company purchased the off-the-shelf 3D processed data, and the interpretation of these data produced a 3D image of the amplitude anomalies previously seen on the 2D lines. A decision was then made to drill a well to verify some of these bright-spots. There was a particular interest for a deep amplitude anomaly at 3.2 sec.

Oryx and Schlumberger Geco-Prakla decided to reprocess the 1995-96 vintage of the 3D data with following objectives: (1) to verify if the results of a 3D AVO processing sequence, based on the common-offset pre-stack time migration (i.e., the COTIM method), could reveal the AVO anomalies associated these bright spots; (2) to compare the results of the 3D AVO processing with those of the 2D AVO processing; (3) and finally, to verify if the 3D AVO processing of a relatively noisy data set could still produce meaningful results for AVO analysis. A 20 square miles area, including the proper migration aperture, was chosen for this reprocessing.

The drilling confirmed that the amplitude anomalies of this prospect correspond to a stack of commercial hydrocarbon accumulations – both shallow and deep.

Acquisition Parameters for the 3D Data

The 3D data set was acquired with the following parameters:

-number of streamers	3
-streamer interval:	160 m
-group interval:	25 m
-number of channels per streamer:	240
-minimum inline offset:	225 m
-maximum offset:	6025 m
-number of sources:	2 (flip-flop)
-source line interval:	80 m
-source point interval:	50 m

The obstructions due to the existing platforms in this area and the presence of a strong feathering of the seismic cables generated a non-uniform subsurface coverage. Two vessels were used to undershoot the obstructions, and a significant amount of infill shooting was required to cover the gaps in the coverage, which however led to excessive folds in some places.

3D AVO Processing Sequence

The challenges of the 3D AVO processing sequence with this data set were several fold, namely noise attenuation, non-uniform subsurface coverage, the imaging of the steep faults, the full use of the 6000m offset information for AVO analysis, and proper amplitude preservation. The processing sequence designed to properly address these issues was based on the COTIM method of the 3D pre-stack migration, and this sequence is described below:

-ambient noise attenuation
-surface-consistent amplitude corrections
-common offset sorting in 20 cubes
-higher- order NMO using the available DMO velocities
-coverage regularization with flexible binning
-wide log-stretch DMO with amplitude and phase calibration
-random noise attenuation in common offset cubes
-interpolation in the cross line direction to generate a bin size of 12.5 m (inline) by 20m (cross line)
-zero offset phase shift migration of the common offset cubes
-sorting to 3D CMP (common-bin) gathers
-backing out the previously applied higher-order NMO
-velocity analysis on 500m by 500m grids
-higher- order NMO with the new velocities
-Q compensation
-phase rotations to match the well synthetics
-generating the pre-stack migrated cube
-common reflection angle decomposition
-generating three common reflection angle stacked cubes: 0-22, 22-44 and 44-60 degrees
-producing AVO attributes

NOISE ATTENUATION

Swell noise was the dominant ambient noise that was encountered on this 3D data set, due to the acquisition in a rough sea-state condition. Isolated spikes and interference from shot-generated noises were also present, but to a small extent. The swell noises were attenuated in the CMP domain where these noises become random in nature. We used a multi-channel statistical measure to identify these noises. The noisy samples were detected as those having amplitudes exceeding a threshold that was determined from the statistical average of amplitudes of the neighboring traces. The detection and the attenuation of the noise samples were made in the selected frequency bands where the noises were present. This procedure for attenuating the swell noise was found very effective in improving the signal to noise ratio. An example of the swell noise attenuation is presented in Figure 1. **Higher--Order NMO**

The standard 2-term hyperbolic NMO equation is generally valid only for small offset ranges. Instead of this hyperbolic equation, , we used a 4-term NMO equation (Taner and Koheler, 1969), to properly handle the non-hyperbolic travel times associated with large offset ranges. An example of CMP gathers which were moveout-corrected using the standard 2-term NMO equation and also using the higher-order 4-term NMO equation is shown in Figure 2. The use of the higher-order NMO equation allowed us to use the larger offsets available in this data set, to preserve amplitude information for angles of incidence up to 60 degrees.

LOG STRETCH DMO WITH AMPLITUDE AND PHASE CALIBRATION

The significant cable feathering due to the strong currents and the obstructions by the existing platforms had a negative impact on subsurface coverage, both on offset and azimuth distributions. DMO processing based on any standard Kirchhoff algorithm is sensitive to non-regular acquisition geometry, and thus could introduce amplitude anomalies that are not at all subsurface related. In our processing, a calibrated log-stretch DMO algorithm (Ronen, 1994) was used, which had the options to compensate for both the amplitude and phase variations generated by an irregular acquisition geometry. Other features of this log-stretch DMO processing that improved our processing results were the 'wide DMO operators' , and the accurate anti-aliasing protection of the operators. The wide DMO operators were effective in regularizing the coverage, because the energy was spread out not only on the line connecting the sources with receivers, but also on the adjacent lines.

COMMON-OFFSET PRE-STACK TIME MIGRATION

The common-offset cubes resulting from NMO-DMO processing were migrated using a zero-offset phase-shift migration algorithm, with appropriate stretch corrections for a laterally variable velocity function that was available in this area. The primary advantages of the zero-phase migration algorithm are several fold, namely, accurate amplitude preservation, accurate imaging of dips up to 90 degrees, good anti-aliasing protection, and more importantly, the high efficiency for speedy processing of a large-volume 3D data. An example of a inline section extracted from the 3D pre-stack migrated volume is shown in Figure 3, which clearly shows a very good definition of a fault trace, that was made possible by the present COTIM method of pre-stack migration.

PROCESSING RESULTS AND DATA ANALYSIS

The results of the 3D AVO processing primarily consisted of the following products: (1) the pre-stack time-migrated stack volume, and (2) the CMP (i.e., common-bin) gathers, (3) the three angle-stack volumes for 0-22, 22-44 degrees and 44-60 degrees, (4) the normal-incidence reflectivity volume (P), the gradient volume (G), the P*G volume and also the P*signG volume. The analyses of all these volumes of data are still in progress, but the preliminary investigation shows

that the present 3D processing sequence reveals the AVO anomalies, ranging from 1.7 to 3.2 seconds, that could be interpreted as indicators for the gas sands. These anomalies, particularly noteworthy being the deep AVO anomaly at 3.2 seconds, which was not present on the 2D AVO processing results, were supported by the drilling results. Figure 4 shows an inline pre-stack migrated section that illustrates the deep amplitude anomaly at 3.2 seconds. The corresponding P*G section showing this anomaly is presented in Figure 5.

CONCLUSIONS

The results of the 3D AVO processing and analysis of the amplitude anomalies over a prospect in the Gulf of Mexico are supported by the drilling results. This example shows that the 3D AVO processing based on a common-offset pre-stack time migration method (COTIM) is able to preserve the subtle amplitude anomalies associated with both shallow and deep targets. Particularly important in this processing sequence was the use of a calibrated log-stretch DMO algorithm to handle the amplitude and phase variations generated by an irregular acquisition geometry

REFERENCES

Ronen, S., 1994, Handling irregular geometry: Equalized DMO and beyond, SEG annual meeting at Los Angeles, Expanded abstracts, 1545-1547

Taner , M.T and Koheler, F., 1969, Velocity spectra, digital derivation and application of the velocity function, Geophysics, vol. 34, 859-872

ACKNOWLEDGMENTS

We acknowledge Schlumberger and Oryx Energy Company for their permission to carry on this study and to present these results

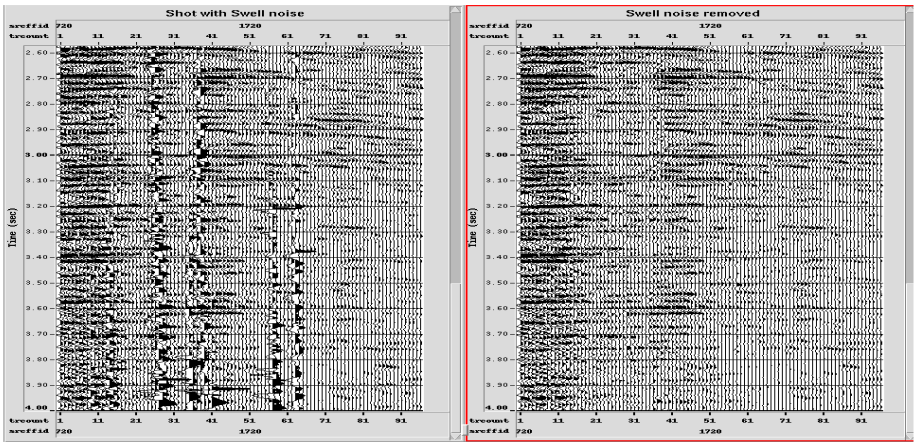

Figure 1: An example of swell noise attenuation in the processed data.

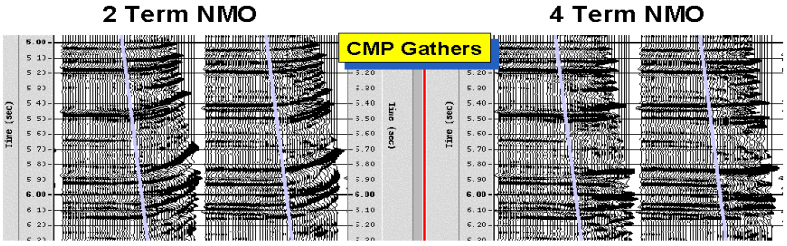

Figure 2: An example of standard (2-term) NMO vs. higher-order (4-term) NMO

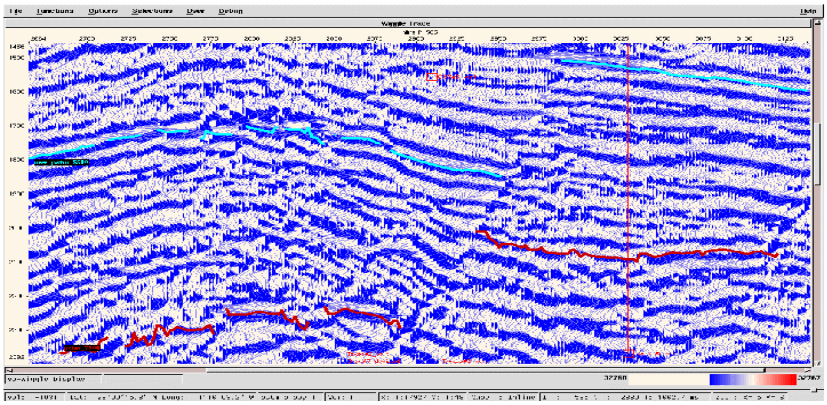

Figure-3: An example of the structural image (i.e. fault) being enhanced by the 3-D PSTM processing.

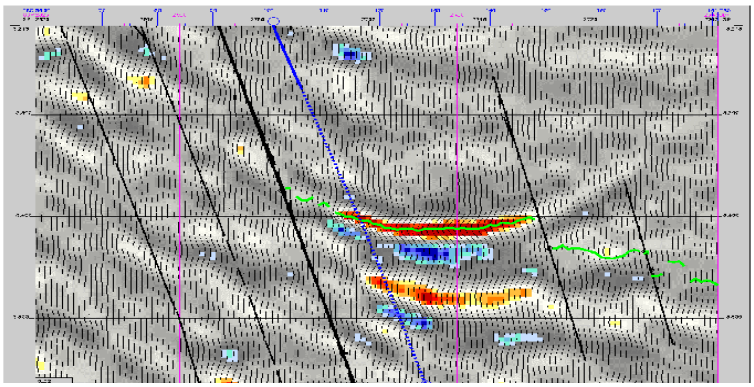

Figure-4: Amplitude anomalies at the deep target (3.2 Seconds)

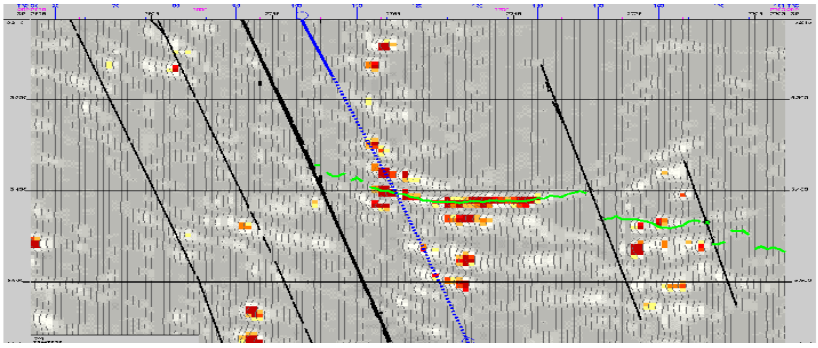

Figure-5: Intercept * Gradient anomalies at the deep target (3.2 Seconds)